Metallurgical and Materials Engineering *Research paper*
Association of Metallurgical Engineers of Serbia AMES https://doi.org/10.30544/840

OPTIMIZATION AND ANALYSIS OF DRY SLIDING WEAR BEHAVIOUR OF N-B_4C/M_OS_2 UREINFORCED AA2219 NANO HYBRID COMPOSITES USING RESPONSE SURFACE METHODOLOGY

Riddhisha Chitwadgi[1], B Siddesh[1], B Latha Shankar[1], R Suresh[2,], N. G Siddeshkumar[3]*

[1] Department of Industrial Engineering and Management, Siddaganga Institute of Technology, Tumkur-572103, Karnataka, India.
[2] Department of Mechanical and Manufacturing Engineering, S. Ramaiah University of applied science, Bengaluru-562054, Karnataka, India.
[3] Department of Mechanical Engineering, Channabasaveshwara Institute of Technology, Tumkur- 572 216, Karnataka, India

Received 11.05.2022
Accepted 25.09. 2022

Abstract

The effect of heat treatment on nano-size B4C particle reinforced hybrid composites is discussed in this paper. For this, hybrid reinforced AA2219 composites with 2% by weight nano B_4C and 2% by weight MoS_2 particulates were fabricated using a two-stage stir casting process, and the specimens were heat treated to assess their influence on wear behavior. Experiments were carried out to study the wear behavior by varying important factors such as aging temperature, load, and sliding distance. Response Surface Methodology (RSM) designed by Box-Behnken was used to identify the critical variables influencing wear rate and optimize wear behavior. To comprehend the wear mechanisms involved, an analysis of the worn surface was presented. Based on the analysis, a regression equation with a predictability of 97.2% was developed for the response to obtain the optimum wear rate. The following order effectively captures the relative importance of the various factors determining the alloy's wear resistance: sliding distance, load, and aging temperature. When compared to load and sliding distance, heat treatments via artificial aging in the temperature range of 200-240 °C have no significant effect on the wear resistance of hybrid AA2219 composites reinforced with n-B_4C and MoS_2 particulates. However, when a temperature range of 200-240 °C is considered, composites exhibit better wear resistance at the aging temperature of 240 °C with ice quenching.

Keywords: AA2219 alloy; B_4C particles; MoS_2 particles; heat treatment; wear rate; response surface methodology.

*Corresponding author: R Suresh, *sureshchiru09@gmail.com*

Introduction

Wear is an important phenomenon to consider when designing mechanical elements found in engines, brake systems, cylinder liners, brake shoes, bearings, and so on. The materials used to make these mechanical components must have a number of characteristics, including high strength, good wear resistance, a consistent coefficient of friction, good temperature stability, corrosion resistance, and effective anti-seizure capabilities [1]. Ceramic reinforced metal matrix composites are promising candidates for meeting these requirements, and thus have a wide range of applications in automotive and aerospace [2, 3]. Particulate metal matrix composite (PMMC) is a better choice than continuously reinforced MMCs for problems such as micro-structural non-uniformity and fiber damage [4-8].

According to research, a typical PMMC frictional pad should have a metallic matrix, particulates, and additives to resist friction. The mechanical, thermal, and corrosion resistance properties of PMMC are influenced by the matrix material used. The hard particles in the PMMC, which are often made of ceramics like $nA1_2O_3$, $nSiO_2$, SiC, B_4C, TiC, Si_3N_4, TiB_2, MgO, and mullite [9], provide better mechanical qualities, wear resistance, and thermal stability. As additives, graphite, MoS2, and boron nitride are used to provide consistent friction, damping, and anti-seizure properties [10-16]. Aluminum-based PMMCs have been widely used in aircraft applications due to their low density, high thermal conductivity, and exceptional corrosion resistance [5, 17]. The aluminum alloy AA2219 is frequently used in rocket fuel tanks and airframe contact components due to its higher specific strength and stiffness, exceptional formability and fracture toughness, excellent cryogenic qualities, and great weldability [18]. Because of their high impact resistance, superior wear resistance, elevated melting point (2450 °C), and low density, B4C nano particles form a reinforcement phase added to AA2219 to improve wear performance [19-20]. Only a few studies have been conducted on B_4C, the third hardest material, and its effects on Al alloy. Lamellar soft MoS_2 particles are added as solid lubricants to the matrix and hard particle reinforcements due to their excellent oxidation resistance, inherent lubricating qualities, and high-temperature stability. They also help to reduce counter surface wear by forming a tribolayer at the contact [21-23].

A variety of operational and material-related variables have been shown in the literature to have a complicated impact on how materials wear [24-28]. In terms of particle size effects on mechanical properties, nano-scale demonstrated remarkable progress through a variety of mechanisms, including grain refinement with particle assistance, particle and dislocation interaction effects, work hardening, elastic modulus mismatch-induced dislocation strengthening, thermal mismatch, and orowan strengthening [29]. In terms of wear resistance, nano size B_4C particle-reinforced AA2024 matrix composites outperformed AA2024 under low load (20 N) and sliding speed (0.6 m/s). The wear resistance of nano-sized B_4C particle reinforced AMMCs was significantly higher than that of micro-sized B_4C particle reinforced AMMCs. Nano particle-assisted grain refining was responsible for the improved wear performance [30]. *Harichandran et al.* conducted a comparison of the wear behavior of micro (70 µm) and nano (80 nm) AA composites reinforced with B_4C [31]. *Alizadeh et al.* reported a similar result for nano B_4C reinforced AA2024 composite fabricated via milling and hot extrusion [32]. *Kumar et al.* investigated the effect of adding lubricant MoS_2 (1.3 µm) particles on micron size B_4C (90 µm) ceramic reinforced AMMCs. The results showed that adding more MoS_2 up to

5% by weight significantly improved the wear resistance of hybrid composites [33]. *Saravanakumar et al.* discovered a similar result for AA2219 [34].

Heat treatment, which is applicable to AMCs, is a heating and cooling technique used on metal to improve mechanical properties. Precipitation hardens as a result of AMC heat treatment. As a result, the mechanical and wear performance of Heat Treated (HT) AMCs outperforms non-HT AMCs [35]. Several studies have been conducted to determine how heat treatment affects the wear and friction characteristics of composites with a specific type of reinforcement, such as alumina. Furthermore, wear and friction characteristics of hybrid composites with two reinforcements have been reported [36]. A few researchers [37-40] worked on wear property modeling, statistical analysis, and optimization. Response Surface Methodology (RSM) is one of the most widely used optimization techniques in the industrial world today [41-45].

The preceding discussion leads to the conclusion that factors such as the influence of different reinforcements, their proportion, size, temperature, processing time, wettability, manufacturing method, and heat treatment (HT) are important in determining the mechanical properties of AMCs. Given the scarcity of wear research on nanoparticle-reinforced AA hybrid composites, there is clearly room to improve wear resistance by combining the addition of nano-ceramic particles and solid lubricant additives in AMCs. The current work is designed for this purpose, as well as to provide a clear understanding of the impact of heat treatment on those composites. The stir casting method was used to produce AA2219/B_4C/MoS_2. The wear behavior of these composites was evaluated at a fixed speed of 3.77 m/s in a variety of aging temperatures (200-240 °C), sliding distances (500-1500 m), and loads (10-50 N).

Experimental Details

Materials Used

In the present study, the matrix used for the preparation of a composite was AA2219 alloy, an Al-Cu binary alloy. Its Chemical composition was obtained using the spectrometer and presented in Table 1.

Table 1. Chemical constituents of AA2219 alloy.

Elements	Mg	Si	Cu	Zr	Fe	Zn	Ti	V	Zn	Al
wt.%	0.02	0.2	5.8-6.8	0.10-0.25	0.30	0.10	0.02-0.12	0.05-0.15	0.1	Balance

Fabrication Method

The nano hybrid AA2219 composites with 2% by weight nano-B_4C and MoS_2 particulates reinforced were created using a two-step stir casting process. A resistance-type electric furnace was used to melt the AA2219 alloy in a graphite crucible at a rate of 5 °C min-1 in a regular air pressure environment. AA2219 was superheated to 750°C and degassed with a tablet of Solid Hexachloro Ethane (C_2Cl_6). A mechanical stirrer coated with Zirconia was used to stir molten metal at 200-250rpm. To avoid moisture and adhering contaminants, the soft MoS_2 and hard n-B_4C nano particles were warmed to 250 °C. To prevent clustering, the n-B4C particles were combined in a 5:2 ratio with the halide salt Potassium Fluoro Titanate (K_2TiF_6). Mixing with the halide salt and vigorous

stirring would improve the particles' ability to remain in contact with the matrix and prevent particle adhesion [46, 47].

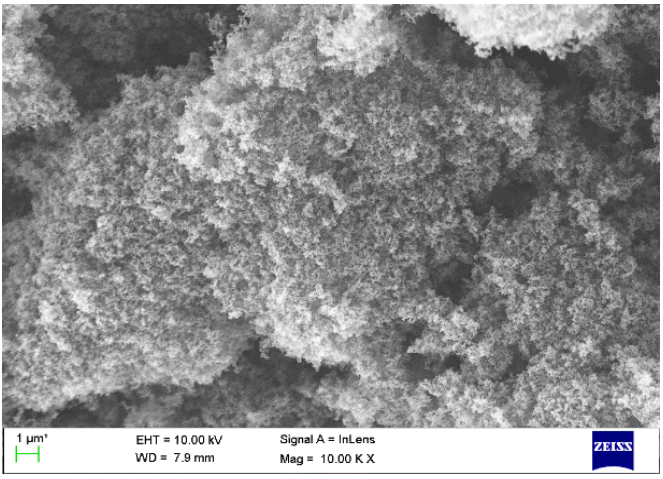

Fig. 1. SEM image of n-B_4C.

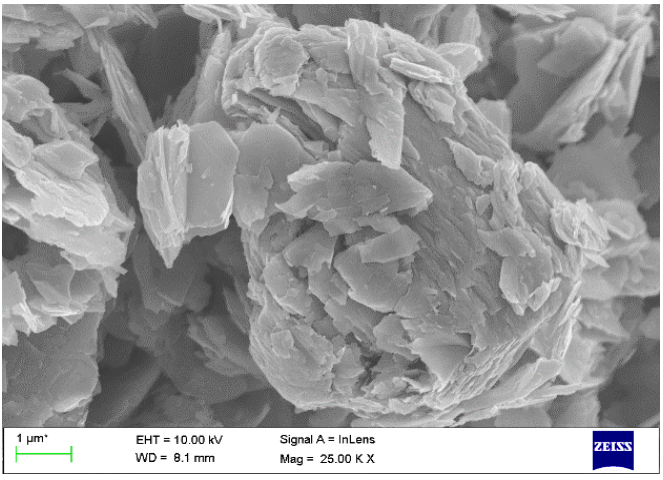

Fig. 2. SEM image of MoS_2.

Finally, the particles were added to the crucible. The hybrid nano composites were created by combining two phases of heated MoS_2 particles and molten metal. The molten AA was combined with the K_2TiF_6 and n-B_4C slurry in the first stage, and the mixture was vigorously stirred at around 225 rpm for 6-8 minutes. The vortex was created in the molten metal in the second stage to facilitate the equivalent distribution of the reinforcements in the matrix, and MoS_2 particles were mixed and aggressively whirled after addition. The molten melt was then poured into a 300 °C pre-heated cast iron die. The cast composites were removed after the mold had reached room temperature in the air. The cast bars were then machined to obtain test samples for microstructural analysis and dry sliding wear performance evaluation. Nano B_4C particles are 30-60 nm in size

and serve as hard ceramic particles, whereas MoS_2 particles are 600-900 nm in size and serve as soft solid lubricant particles. Figures 1 and 2 show the microstructures of n-B_4C and MoS_2 particles, respectively.

Age-hardening of composites

The composites were heat treated using an age-hardening process. Age-hardening took place at a high temperature here. As a result, the technique is referred to as artificial age-hardening. The age hardening process was carried out in a Mufle furnace at three different temperatures: 200 °C, 220 °C, and 240 °C. After reaching the required temperature, the samples were immersed for 24 hours before being air cooled.

Wear test

Figure 3 depicts the pin on disc device and wear test rig used in the current work. A pin-on-disc tribometer was used to perform the dry sliding wear test (TR 2OLE-PHM-400 model). A revolving steel disc with a diameter of 120 mm made of EN-31 grade steel was tested against age-hardened pin-shaped test specimens with a diameter of 8 mm and a height of 30 mm. The chemical composition of the steel disc was as follows (in weight percent): C is 0.15 percent, Mn is 0.8 percent, Si is 0.26 percent, S is 0.04, P is 0.04 percent, and Fe is the remainder. The tensile strength of the disc was 430 MPa, the hardness was 62 HRC, and the surface roughness was 1.6 Ra.

All of the wear tests were carried out with no lubrication. The dry sliding wear testing was carried out in accordance with ASTM G 99-05 specifications. Following each run, the samples were cleaned with ultrasonic acetone, dried, and their weight was determined using a digital scale (METTLER, precision: 0.01 mg). The composites' specific wear rate (mm^3/N-m) was calculated by dividing mass loss (g) by density (g/mm^3), then by the product of sliding distance (m) and normal load (N). The wear surface of the composite was investigated at different sliding distances, aging temperatures, and load conditions. After running each test three times, the results were averaged.

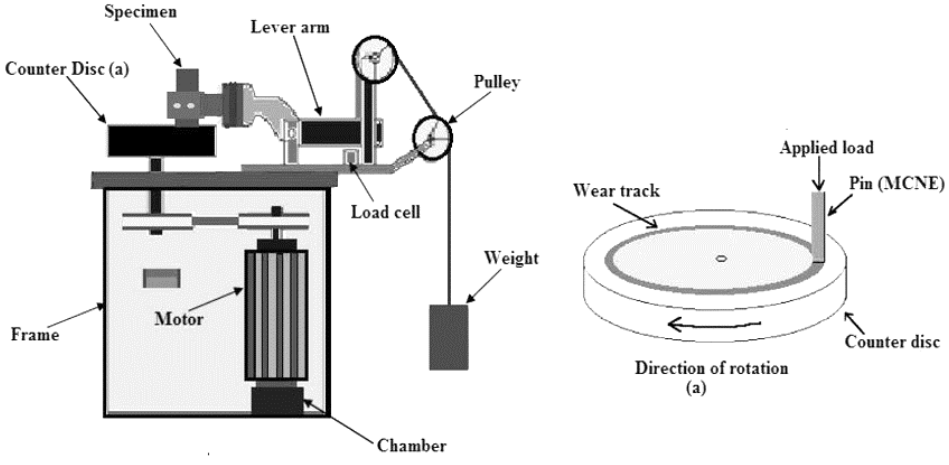

Fig. 3. Schematic image of Pin-on-disc tribometer apparatus.

Results and Discussion

Microstructure analysis

The microstructure of the matrix material is shown in Fig. 4 to have a fairly uniform distribution of B_4C particles and a random distribution of MoS_2 reinforcing particles. This effectively demonstrates the nano hybrid composites produced by the stir casting technique.

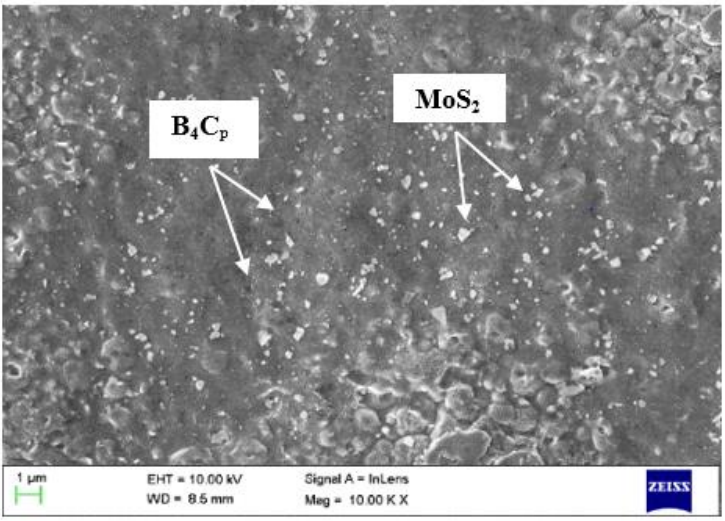

Fig. 4. AA2219+2% B_4C+2% MoS_2 Nano hybrid composite.

Response Surface Methodology

RSM uses math and statistics to model, improve, and optimize the response variable with the fewest number of experiments [48]. Despite the fact that the traditional method of experiment design necessitates extensive resource consumption, assessing the combined effects of applicable components is difficult. In previous work [20], a thorough explanation of factor selection was provided, and it was concluded that, of the four factors considered, sliding speed has the least effect on wear rate. As a result, the least significant factor was removed from the current work, and because this work focuses on the influence of ageing temperature on wear behavior, it was decided to consider the important factors as load, sliding distance, and ageing temperature. The Box Behnken Design with three levels of each factor is chosen from among the popular RSM designs for fitting second order polynomials to response surfaces. To estimate the experimental error for the three variables chosen and three levels, the design required 15 experiments with 12 factorial points and three centering points for replication. Table 2 shows the factors and levels used in the experiment, and the experiment was carried out in accordance with the design matrix's run order, which is shown in Table 3.

At the end of each experiment, all three parameter values were adjusted and reset for the next run. This was done to create unpredictability caused by errors in experimental

settings [49, 50]. The link is predicted using a second-order polynomial regression model, the general form of which is shown in Equation 1:

$$Y = \beta_0 + \sum_{j=1}^{k} \beta_j X_j + \sum_{j=1}^{k} \beta_{jj} X_j^2 + \sum_i \sum_{<j=2}^{k} \beta_{ij} X_i X_j + e_i \quad 1$$

Where, Y on left hand side of the equation gives value of dependent variable; X_i and X_j denote independent variables; β_0 is intercept coefficient; β_j, β_{jj}, and β_{ij} are interaction coefficients; k gives number of independent factors and equal to 3 in this case; and error is denoted by e_i [51]

Table. 2. Factors and respective levels used in this experimental study.

Factor	Unit	Factor Level		
		-1	0	+1
Aging Temperature	^oC	200	220	240
Load	N	10	30	50
Sliding distance	m	500i	1000	1500

Main Effect Plot

The main effect plot is shown in Fig. 5, and it can be seen that as the ageing temperature rises from 200 °C to 240 °C, the wear rate decreases. Wear rate, on the other hand, increases as both the sliding distance and the applied force increase. It demonstrates that the factors that have the greatest influence on wear behavior are load, ageing temperature, and sliding distance. Furthermore, the main effect plot clearly shows that the process variables that result in the lowest wear rate are the lowest load (10 N), shortest sliding distance (500 m), and maximum ageing temperature (240 °C).

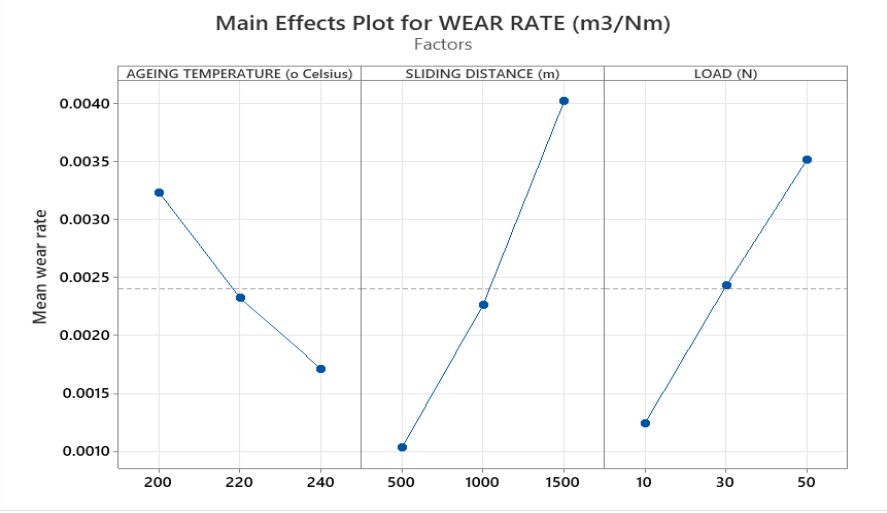

Fig. 5. Main Effect Plot for Wear rate.

Table 3. Design Matrix for conducting wear tests.

Std Order	Run Order	Heat treatment	Sliding Distance	Load	Experimental Wear rate	Predicted Wear rate	Error (%)
1	1	-1	-1	0	0.00316798	0.0032961	-3.88789
2	2	+1	-1	0	0.00207593	0.0021776	-4.6689
11	3	0	-1	+1	0.00019886	0.0002016	-1.33955
14	4	0	0	0	0.002289	0.002351	-2.63718
13	5	0	0	0	0.00229958	0.0022178	3.689308
6	6	-1	0	-1	0.005336	0.0055059	-3.08578
9	7	0	-1	-1	0.0031234	0.0029947	4.297592
10	8	0	+1	-1	0.00146293	0.0015316	-4.48355
3	9	-1	+1	0	0.0019896	0.0020208	-1.54394
4	10	+1	+1	0	0.00215725	0.0021776	-0.93452
7	11	-1	0	+1	0.0005717	0.0005447	4.95493
15	12	0	0	0	0.005413074	0.0052298	3.504417
5	13	-1	0	-1	0.000545729	0.0005205	4.847109
8	14	+1	0	+1	0.00169952	0.0016375	3.787481

Analysis of Variance

The parameters' relevance in the created model was evaluated using the ANOVA approach. According to the determination coefficient (R^2), which measures the model's goodness of fit [52], only a small portion of the overall variance—less than 5%—is not assessed by the model. A higher adjusted determination coefficient value indicates that the observations are better fit (adjusted R^2 = 92.13 percent). The model is statistically significant because its p-value is less than 0.05 [60-63]. The three main characteristics are identified as sliding distance, load, and aging temperature, which contribute 50.15 percent, 29.04 percent, and 13.05 percent, respectively (Table.4).

Table.4. ANOVA table of wear rate.

Source	DF	Sum of Sq.	Contribution	Mean Sq.	F-Value	P-Value	Significant/ Insignificant
Model	9	$3.953x10^{-5}$	97.19%	$4.103x10^{-6}$	19.20	0.002	Significant
Aging Temperature	1	$5.112x10^{-6}$	13.05%	$5.112x10^{-6}$	23.20	0.005	Significant
Sliding Distance	1	$18.1x10^{-6}$	50.15%	$18.1x10^{-6}$	89.18	0.0001	Significant
Load	1	$10.03x10^{-6}$	29.04%	$10.03x10^{-6}$	51.65	0.001	Significant
Aging Temperature *Aging Temperature	1	$1.032x10^{-6}$	0.23%	$1.032x10^{-6}$	0.52	0.503	
Sliding Distance *Sliding Distance	1	$1.012x10^{-6}$	0.79%	$1.012x10^{-6}$	1.38	0.292	
Load* Load	1	$1.023x10^{-6}$	0.00%	$1.023x10^{-6}$	0.00	0.948	

Aging Temperature *Sliding Distance	1	$1.113x10^{-6}$	1.43%	$1.113x10^{-6}$	2.53	0.172
Aging Temperature *Load	1	$1.003x10^{-6}$	0.31%	$1.003x10^{-6}$	0.55	0.491
Sliding Distance * Load	1	$1.103x10^{-6}$	2.19%	$1.103x10^{-6}$	3.89	0.106
Lack-of-Fit	3	$1.123x10^{-5}$	2.74%	$1.003x10^{-6}$		0.058
Pure Error	2	$1.002x10^{-6}$	0.07%	$1.002x10^{-6}$		
Total	14	$5.176x10^{-5}$	100.00%			

**R-Sq = 97.19% R-Sq(adj) = 92.13%*

Surface Plots

The effect of aging temperature and sliding distance on wear rate at a load of 30 N is shown in Fig. 6. It can be seen that as the sliding distance increased, so did the wear, which was already discussed in the previous section. However, heat treatment tends to reduce wear, and the lowest wear rate is observed at the maximum aging temperature. Figure 7 depicts the effect of load and sliding distance on wear rate at 220 °C aging. The wear increased with the increase in load, which could be explained by the fact that as the load increases, high pressure is applied to the sliding surfaces, causing the composites to wear out faster. Greater sliding distance also increases wear rate because the interaction time between the sliding surfaces increases, resulting in more material loss. Evidence from the literature suggests that the combined action of load and sliding distance exacerbated wear [53]. Similar findings have been found in the literature, and the factors that contribute to these findings include an increase in temperature and asperity breakup, welding of the pin with the disc, and frictional coefficient on the surface of the composites, softening the matrix materials [54].

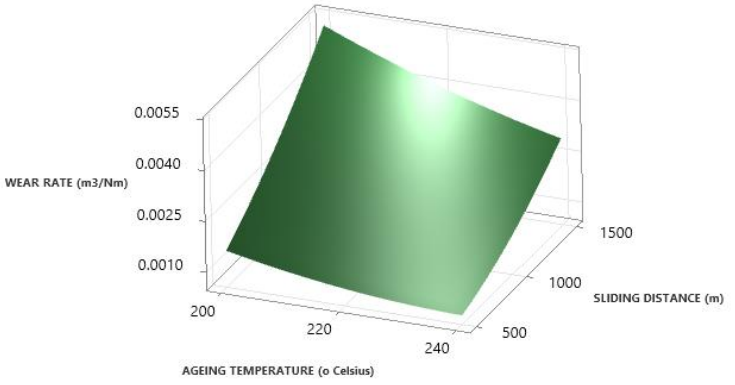

Fig. 6. Surface Plot of the wear rate against Sliding distance and Aging temperature.

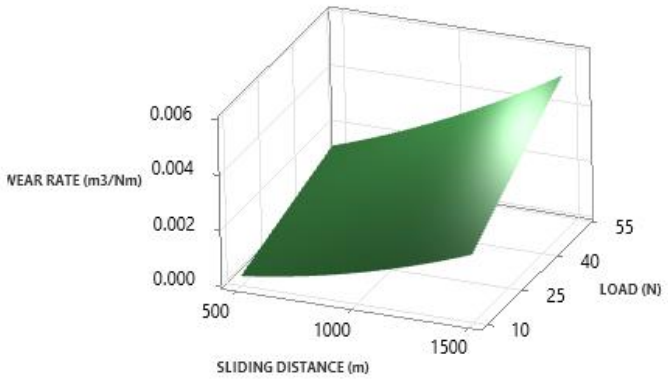

Fig. 7. Surface Plot of the wear rate against Sliding distance and Load.

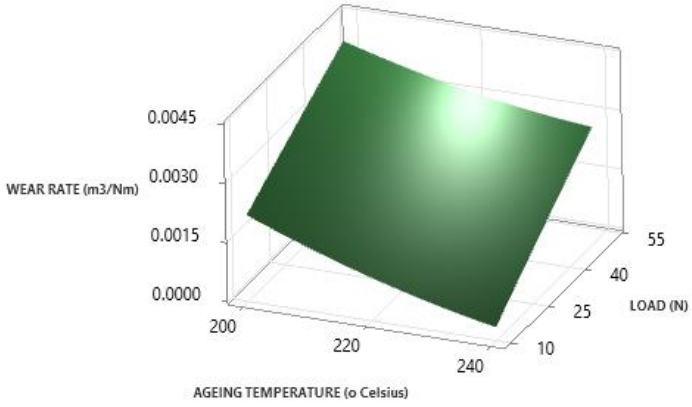

Fig. 8. Surface Plot of the wear rate against aging temperature and load.

The impact of load and ageing temperature on wear rate at 1000 m of sliding distance is depicted in Fig. 8. The wear rate increased as the load increased, and the opposite trend was observed as the aging temperature increased.

Checking of adequacy of model

The normal probability curve of the wear rate residuals for the nano hybrid metal matrix composite is shown in Fig. 9. Because the residuals are seen in a straight line, it shows a normally distributed distribution of errors. A graph for the run order and residuals for wear rate was created to determine the data's independence and demonstrate that there was no discernible trend.

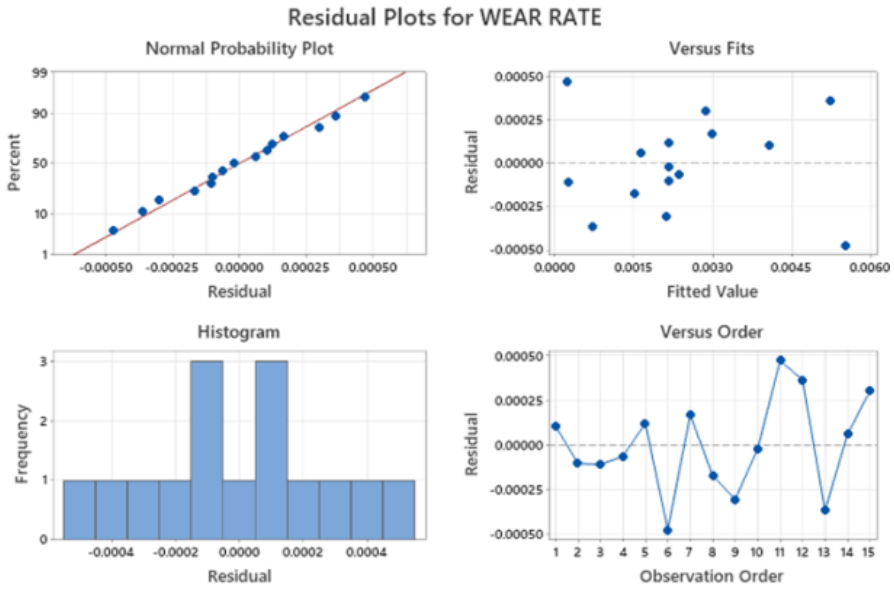

Fig. 9. Analysis of Input data for AA2219 nano composites.

Correlation with Regression analysis

Regression analysis was done to assess the wear rate and **Error! Reference source not found.** gives the second-order polynomial regression equation it provided for wear rate.

*Wear Rate = 0.024 - 0.0002 Ageing Temperature + 0.000007 Sliding Distance - 0.000076 Load + 0.0000001 Ageing Temperature * Ageing Temperature + 0.00000020 Sliding Distance * Sliding Distance - 0.00000010 Load * Load - 0.00000020 Ageing Temperature * Sliding Distance + 0.00000020 Ageing Temperature * Load + 0.00000030 Sliding Distance * Load (2)*

Optimization

Since the study has its base on the concept that "smaller the better," the hybrid composite with the minimum wear rate will be regarded as ideal. Multi-response prediction was used to determine the best values for the lowest wear rate, as shown in Fig. 10. The best conditions for the lowest wear rate are clearly found to be a sliding distance of 500 m, a load of 10 N, and an aging temperature of 240 °C.

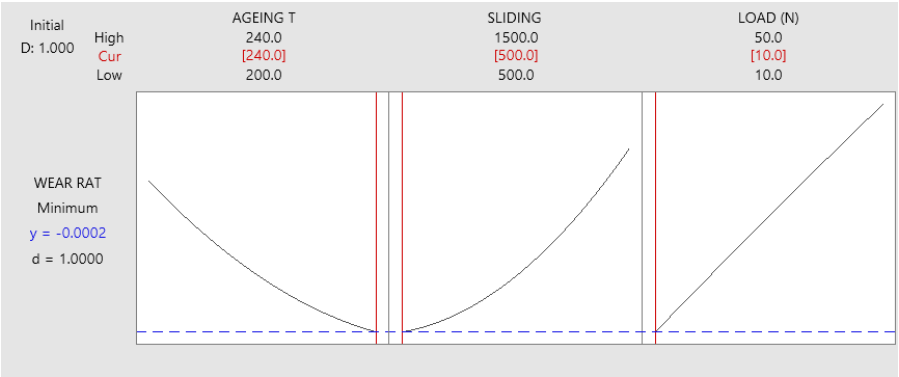

Fig. 10. Results of response optimizer.

As shown in the wear rate main effect plots (Fig. 5), composites aged at 240 °C have improved wear resistance, and subsequent ice quenching reduces the high wear rate. Heat-treated composites have higher hardness when compared to unheated composites. The reason for this could be that a much harder intermetallic phase has formed, and ice quenching improves composite hardness by stabilizing the intermetallic phase [20]. Both quenching conditions resulted in changes in wear resistance. Water quenching has significantly reduced the wear rate of hybrid composites. Composite materials showed a greater reduction in wear rate after being quenched in ice cubes. All of this suggests that heat treatment has an effect on composite wear behavior, which is consistent with previous findings from other experiments [40]. In this case, the oxide coating that forms on the surface of the composite prevents metal contact, lowering the wear rate of heat-treated MMCs in comparison to unheated ones. The particles in heat-treated composites help to reduce the severity of wear [38].

Analysis of Wear and Wear debris

SEM images were used to examine the wear-related damages to the composite pin under various load, aging temperature, and sliding distance conditions. Figures 11 through 14 show the wear mechanism of hybrid AA2219 composites. The main wear mechanisms, according to the literature, are adhesion, particle pull-out, and abrasion [38]. To demonstrate the composite's abrasion wear, grooves parallel to the sliding direction were created in Fig. 11. Hard asperities of the steel counter face, caused by abrasion, plough into the pin and remove small fragments of material [55, 56]. Ploughing causes material displacement on either side of the abrasion groove or wedge formation [57].

As the load increases, the counter-face material's hard asperities dig deeper into the softer face of the pin, causing significant plastic deformation and the dispersal of wear debris across the surface. The pattern of increased wear intensity with increasing load is consistent with the findings of other researchers [53, 54, 58-60]. For higher loads and longer sliding distances, the stress concentration occurs at the pointed edges of reinforcement particles, which initiate fractures in the matrix next to them. This contributes to the formation of debris. As a result, when sliding in a dry environment at higher loads, the debris accumulated between the sliding surfaces ploughs the surfaces of the pin, severely wearing them down, as illustrated in Fig. 11. Figure 12 depicts spalls,

pits, and cracks, while Figures 13 and 14 depict surface oxidation caused by adhesive wear. The flaky debris can be seen in the SEM images, and the pores in the worn surface show signs of abrasive wear. Numerous experts have noted that by confining wear debris inside the pores and reducing particle aggregation, pores may even improve wear resistance. The wear debris from the removed oxide layer fills the grooves on the surface of the pin, preventing metal-to-metal contact.

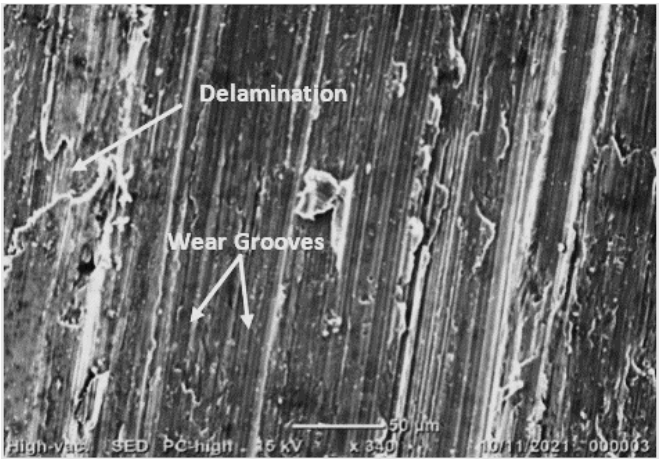

Fig. 11. SEM images of worn out surfaces tested at sliding velocity of 3.77 m/sec, sliding distance of 1500 m and 10 N load.

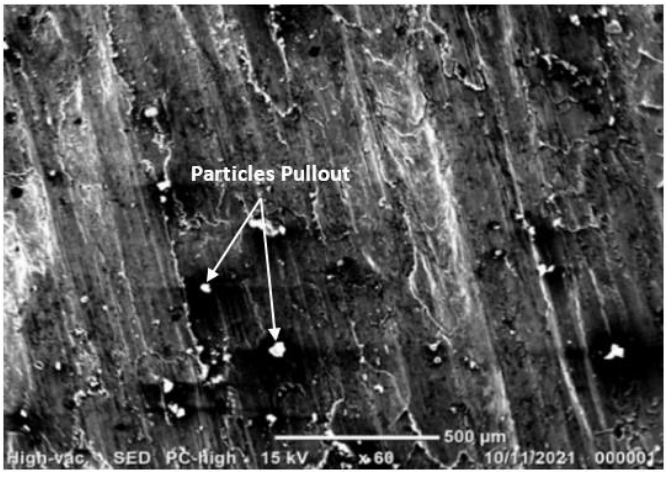

Fig. 12. SEM images of worn out surfaces tested at sliding velocity of 3.77 m/sec, sliding distance of 1500 m and 30 N load.

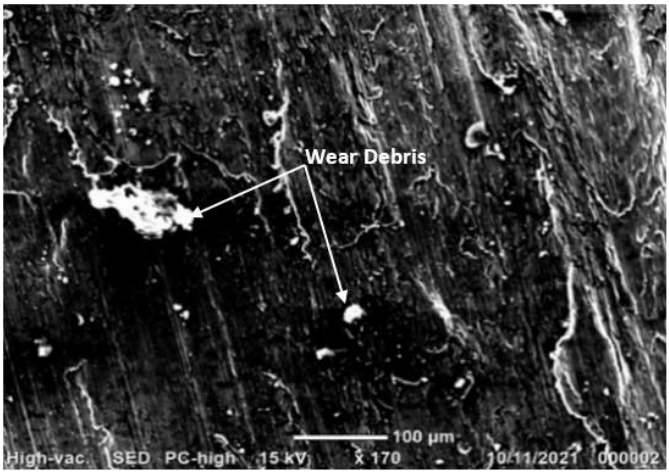

Fig. 13. SEM images of surfaces worn out and tested at sliding velocity of 3.77 m/sec, sliding distance of 1500 m and due to adhesive wear.

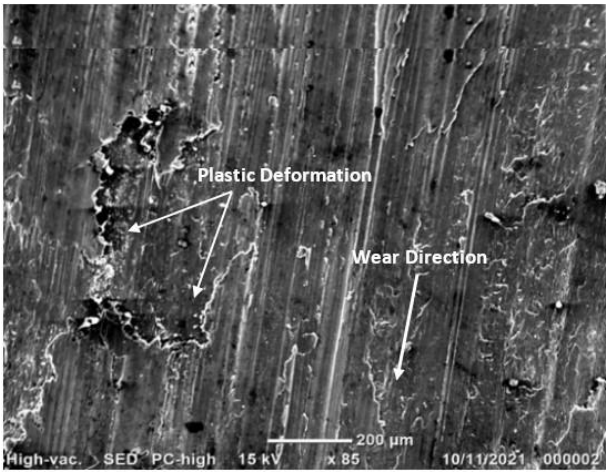

Fig. 14. SEM images of surfaces worn out and tested at sliding velocity of 3.77 m/sec, sliding distance of 1500 m and 50 N load.

Aging Effect

The inclusion of ceramic particles in the matrix improves the materials' hardness, wear resistance, thermal stability, and durability. When composite was aged at 200 °C, it exhibited significantly different wear behavior than when aged at 240 °C. The wear rate of fine-grained reinforced composites was much lower than that of coarse-grained reinforced composites at 200 °C and higher load. According to the shape of the wear track and debris, surface damage is primarily caused by the formation of fractures surrounding the vacuum on the particle-particle interface [61-64]. Aging is critical for improving the wear resistance, hardness, thermal stability, and microstructure of hybrid composites.

Conclusions

These are the main inferences that may be made from the research at hand:

- The traditional stir casting method was effectively used to fabricate the hybrid AA2219 composites, and assessment of the microstructure demonstrated that the reinforcing particles (B_4C and MoS_2) are distributed pretty uniformly in matrix material.
- The importance of the various elements influencing the alloy's wear resistance can be presented in the following order: 1. Sliding distance, 2. Load, and 3. Aging temperature. This shows that heat treatments through artificial aging in the temperature range of 200-240 °C do not influence substantially the wear resistance of hybrid AA2219 composites reinforced with nano B_4C and MoS_2 particulates each added at 2% by weight, when compared to load and sliding distance. A similar result was reported in the literature for other aluminum alloy composites (6, 64). When the range of 200-240 °C is considered, at the aging temperature of 240 °C with ice quenching, composites exhibit better wear resistance.
- Examinations of the worn pin surfaces reveal signs of abrasion and other wear processes, particle pull-out, adhesion, and oxidation.
- The regression-based equation is dependable to estimate the wear rate with an accuracy of 92 %, and the relationship between the projected and measured wear rate is extremely excellent with a +5% error. These results show that the model has a reasonable level of precision in its ability to describe the wear data.

References

[1] J.D. Kim, H.J. Kim, S.W. Koh: Materials science forum, 510 (2006) 234-237.
[2] S. Suresha, B.K. Sridhara: Materials & Design, 31 (2010) 1804-1812.
[3] C. Velmurugan, R. Subramanian, S.S. Ramakrishnan, S. Thirugnanam, T.Kannan, B. Anandavel: Industrial Lubrication and Tribology, 66 (2014) 545-554.
[4] M.E. Smagorinski, P.G. Tsantrizos, S. Grenier. A. Cavasin, T. Brzezinski, G. Kim:Mater. Sci. Eng. A, 244 (1998) 86-90.
[5] A.H. Gurcan, T.N. Baker: Wear, 188 (1995) 185-191.
[6] A. Martin, M.A. Martinez, J.L. Lorca: Wear, 193 (1996)169-179.
[7] S. Wilson, A.T. Alpas: Wear, 196 (1996) 270-278.
[8] H. Zhu, H. Wang, L. Ge: Wear, 264 (2008) 967-972.
[9] F.E. Kennedy, A.C. Balbahadur. D.C. Lashmore: Wear, 203 (1987) 715-721.
[10] K. VijayaBhaskar, S. Sundarrajan, B. Subba Rao, K. Ravindra, In: Proceedings Materials today, 2018, p.5891.
[11] Yang, Yi-long, Yun Zhang, Hao-ming Zhang, Xu-he Liu, Xiao-qian Li: Journal of Central South University, 29(2022)767-779.
[12] A.S Aravanakumar, L. Rajeshkumar, D. Balaji, M.P. JithinKarunan: Arabian Journal for Science and Engineering, 45 (2020)9549-9557.
[13] A. Saravanakumar, S. Sivalingam,L. Rajeshkumar, In: Proceedings Materials Today, 2020, p.8321.
[14] B. LathaShankar, P.M. Nagaraj, K.C. Anil, In: Proceedings Materials Today, 2017, p.10739.
[15] N. Natarajan, S. Vijayarangan, I. Rajendran: Wear, 261 (2006) 812-822.
[16] R.K. Uyyuru, M.K. Surappa, S. Brusethaug: Wear, 260 (2006) 1248-1255.

[17] S.R.K. Rao, G.M. Reddy, K.S. Rao, P.S. Rao, M. Kamarai, K.P. Rao In: Proceedings Trans. Indian Inst. Met., 57(2004) 451-459.
[18] V. Bhuvaneswari, L. Rajeshkumar, K.N.S. Ross: Journal of Materials Research and Technology, 15 (2021) 2802-2819.
[19] M. Khakbiz, F. Akhlaghi: Journal of Alloys and Compounds, 479(2009) 334-341.
[20] N.G. SiddeshKumar, T. RamPrabhu, G.S. ShivaShankar, S. Basavarajappa: Tribology-Materials, Surfaces & Interfaces, 10 (2016) 138-149.
[21] P. Radha, N. Selvakumar, R. Harichandran: Archives of Metallurgy and Materials, 64 (2019) 1163-1173.
[22] X. Shi, Z. Xu, M. Wang, W. Zhai, J. Yao, S. Song. A.Q. udDin, Q. Zhang: Wear, 303 (2013) 486-494.
[23] L. Das, M. Aggarwal, K. Rajkumar, S. Aravindan, M. Gupta: Tribology transactions, 55 (2012) 334-344.
[24] J.M. Mistry, P.P. Gohil: Composites Part B: Engineering, 161 (2019) 190-204.
[25] H. Nieto, L. Yang, J.M. Jiang, Schoenung: Wear, 390(2017) 228-235.
[26] G. Dixit, M.M. Khan: Jordan Journal of Mechanical & Industrial Engineering, 8 (2014)351-358.
[27] P.D. Srivyas, M.S. Charoo, In: Proceedings, Materials Today, 2018, p.20041-53.
[28] V.M. Ravindranath, G.S. Shiva Shankar, S. Basavarajappa, N.G. Siddesh Kumar, In: Proceedings Materials Today, 2017, p.11163-1116.
[29] Z. Zhang, D.L. Chen: Materials Science and Engineering: A, 483(2008) 148-152.
[30] A. Abdollahi, A. Alizadeh, H.R. Baharvandi: Materials & Design, 55(2014) 471-481.
[31] R. Harichandran, N. Selvakumar: Archives of civil and mechanical engineering, 16(2016) 147-158.
[32] A. Alizadeh, E. Taheri-Nassaj: Materials characterization, 67(2012) 119-128.
[33] N.G. Siddeshkumar, G.S. Shiva Shankar, S. Basavarajappa: Applied Mechanics and Materials, 766 (2015) 219-228.
[34] Saravanakumar, V. Bhuvaneswari, G. Gokul: Materials Today Proceedings, 27 (2020) 2645-2649.
[35] J.M. Mistry, P.P. Gohil: Science and Engineering of Composite Materials, 25 (201 8) 633-647.
[36] D. Jun, L. Yaohui, Y. Sirong, L. Wenfang: Wear, 262 (2007), 1289-1295.
[37] K. Mahadevan, K. Raghukandan, T. Senthilvelan, B.C. Pai, U.T.S. Pillai: Journal of materials processing technology, 171 (2006)314-318.
[38] S. Basavarajappa, Chandramnohan, J. PauloDavim: Materials & Design, 28 (2007) 1393-1398.
[39] S.S. Mahapatra, A. Patnaik: Materials & Design, 30 (2009) 2791-2801.
[40] S. Koksal, F. Ficici, R. Kayikci, S.O. Sava: Materials & Design, 42 (2012) 124-130.
[41] N. Mandal, H. Roy, B. Mondal, N.C. Murmu, S.K. Mukhopadhyay: Journal of Materials Engineering and Performance, 21 (2012) 17-24.
[42] Baradeswaran, A. Elayaperumal, R.F. Issac In: Proceedings Procedia Engineering, 2013, p.973.
[43] P.V. Reddy, P.R. Prasad, D.M. Krishnudu, E.V. Goud: Journal of Bio-and Tribo-Corrosion, 5 (2019)1-10.
[44] G.T. Danappa, C.R. Raghavendra, R.P. Swamy, K. Naik, In: Proceedings Materials Today, 2021, p.2797-2802.

[45] A. Gudimetla, D. Lingaraju, S.S. Prasad: CompositesTheory and Practice, 21(2021) 3-11.
[46] K. Kalaiselvan, N. Murugan, Siva Parameswaran: Materials & Design, 32 (2011) 4004-4009.
[47] F. Toptan, A. Kilicarslan, Kerti: Materials Science Forum 636 (2010) 192- 197.
[48] S.C. Vettivel, N. Selvakumar, R. Narayanasamy, N. Leema: Materials & Design, 50 (2013) 977-996.
[49] P. Harris, B.L. Smith: Metal Construction, 15 (1983) 661-666.
[50] T. Kannan, N. Murugan: Journal of Materials Processing Technology, 176 (2006) 230-239.
[51] I. Khuri, J.A. Cornell: Response Surfaces Design and Analysis, 2nd ed., Marcel Dekker Inc., New York, 1996.
[52] D.C. Montgomery: Design and analysis of experiments, 10th ed., Wiley, 2019.
[53] [53] P. Sharma, D. Khanduja, S. Sharma: Journal of Materials Research and Technology, 5 (2016) 29-36.
[54] [54] R. Saraswat, A. Yadav, R. Tyagi, In: Proceedings Material Today 2018, p.16963-72.
[55] [55] A.M. Hassan, G.M. Tashtoush, J.A. Al-Khalil: Journal of composite materials, 41 (2007)453-65.
[56] [56] Y. Sahin, M. Acilar: Composites Part A: Applied Science and Manufacturing, 34 (2003)709-718.
[57] [57] S. Wilson, A.T. Alpas: Wear, 196 (1996) 270-278.
[58] [58] N. Idusuyi, J.I. Olayinka: Journal of Materials Research and Technology, 8 (2019) 3338-3346.
[59] [59] B.M. Viswanatha, M.P. Kumar, S. Basavarajappa, T.S. Kiran: Tribology in Industry, 36 (2014) 40-48.
[60] [60] A.M. Rajesh, M.K. Kaleemulla, S. Doddamani: Tribology in Industry, 41 (2019) 344-354.
[61] [61] S. Baskaran, V.A. Anandakrishnan, M. Duraiselvam: Materials &Design, 60 (2014)184-192.
[62] [62] S. Balaji, P. Maniarasan, S.V. Alagarsamy, P. Raveendran, In: Proceedings Materials Today, 2021, p. 2214
[63] [63] N.G. Siddeshkumar, G.S. Shiva Shankar, S. Basavarajappa: Applied Mechanics and Materials, 766 (2015) 219-228.
[64] [64] G. B. Veeresh Kumar, C.S.P. Rao, N. Selvaraj: Journal of Minerals and Materials Characterization and Engineering, 10 (2011) 59-91.